

OPTIMAL HEAT TRANSFER AND OPTIMAL EXIT TIMES*

FLORENCE MARCOTTE[†], CHARLES R. DOERING[‡], JEAN-LUC THIFFEAULT[§],
AND WILLIAM R. YOUNG[¶]

Abstract. A heat exchanger can be modeled as a closed domain containing an incompressible fluid. The moving fluid has a temperature distribution obeying the advection-diffusion equation, with zero temperature boundary conditions at the walls. Starting from a positive initial temperature distribution in the interior, the goal is to flux the heat through the walls as efficiently as possible. Here we consider a distinct but closely related problem, that of the integrated mean exit time of Brownian particles starting inside the domain. Since flows favorable to rapid heat exchange should lower exit times, we minimize a norm of the exit time. This is a time-independent optimization problem that we solve analytically in some limits and numerically otherwise. We find an (at least locally) optimal velocity field that cools the domain on a *mechanical* time scale, in the sense that the integrated mean exit time is independent on molecular diffusivity in the limit of large-energy flows.

Key words. heat transfer, exit time distribution, mixing enhancement

AMS subject classifications. 76R05, 65K10

DOI. 10.1137/17M1150220

1. Introduction. Optimizing the heat transfer from a bounded domain toward the ambient exterior is a critical issue in a wide range of engineering problems where a fluid is used to cool down (or warm up) a space of interest. Applications typically span from the ventilation of buildings [15, 7, 4] to the cooling of microprocessors [12, 26]. An example of particular concern in the last decade is the efficient cooling of computing equipment in data centers [18, 5, 11], whose energy budget in the United States alone represented about 1.8% of the country’s overall electricity consumption in 2014 [3]. Enhancement of heat transfer by capillary or convective motion, whether natural or forced, can be achieved, for example, by tailoring the geometry of the heat exchanger domain [7, 4] or the physical properties of the cooling fluid [6]. Much of the current progress in designing industrial heat exchanger devices relies on direct numerical simulations in complex flows and geometries [16]. In a more theoretical context, flow patterns have been optimized to improve Rayleigh–Bénard convection [21, 28] or to achieve maximal heat transport in simple two-dimensional (2D) geometries [8, 25, 2, 1]. The optimal distribution of sources and sinks has also been investigated for optimal transport of a passive scalar, whether heat or tracer [20, 24, 22].

*Received by the editors October 2, 2017; accepted for publication (in revised form) January 5, 2018; published electronically February 20, 2018.

<http://www.siam.org/journals/siap/78-1/M115022.html>

Funding: This work was partly supported by US National Science Foundation award OCE-1332750 and the Office of Naval Research. The first author was supported by a Geophysical Fluid Dynamics Fellowship. The second author’s work was supported by US National Science Foundation award DMS-1515161 and a fellowship from the John Simon Guggenheim Foundation.

[†]Laboratoire de RadioAstronomie, Département de Physique, Ecole Normale Supérieure, 24 rue Lhomond, 75005 Paris, France, and Institut de Physique du Globe de Paris, 1 rue Jussieu, 75005 Paris, France (florence.marcotte@dalembert.upmc.fr).

[‡]Center for the Study of Complex Systems, Department of Mathematics and Department of Physics, University of Michigan, Ann Arbor, MI 48109 (doering@umich.edu).

[§]Department of Mathematics, University of Wisconsin–Madison, Madison, WI 53706 (jeanluc@math.wisc.edu).

[¶]Scripps Institution of Oceanography, University of California San Diego, La Jolla, CA 92093 (wryoung@ucsd.edu).

In its simplest form, a heat exchanger is a device designed to transfer heat between a fluid and some heat source, either for cooling or for heating. Its operation can be modeled as the advection and diffusion of a passive concentration of heat $c(x, t)$:

$$(1) \quad \frac{\partial c}{\partial t} = -u \cdot \nabla c + \kappa \Delta c, \quad \nabla \cdot u = 0,$$

where $u(x)$ is the steady incompressible advecting flow transporting heat throughout the domain $\Omega \subset \mathcal{R}^d$, and κ is the thermal diffusivity. We treat the flow as given, i.e., it does not obey any particular equation of motion but is rather under our control subject to energy constraints discussed below. We shall sometimes refer to c as temperature, since heat and temperature are assumed to be related by a constant heat capacity.

Without loss of generality, we impose the initial and boundary conditions

$$(2) \quad c(x, 0) = c_0(x) \geq 0, \quad c = 0 \text{ and } u \cdot n = 0 \text{ on } \partial\Omega,$$

where n is the outward unit normal to the boundary. Thus the interior of Ω contains warm fluid while the exterior world is at zero temperature. The goal of the heat exchanger flow is to reduce the amount of heat in Ω , i.e., to cool the fluid, as rapidly as possible. In this paper we will examine optimal solutions to this heat exchange problem, which means designing flows u with superior transport properties.

The total amount of heat in Ω is the integrated concentration $\langle c \rangle$:

$$(3) \quad \langle c \rangle(t) = \int_{\Omega} c(x, t) d\Omega.$$

Angle brackets will denote an integral over Ω . After integrating (1) and using (2), we have

$$(4) \quad \frac{\partial}{\partial t} \langle c \rangle = \kappa \int_{\partial\Omega} \nabla c \cdot n dS \leq 0.$$

The rate of change of $\langle c \rangle$ is dictated by the heat flux at the boundary. The role of the advecting flow—which does not appear explicitly in (4)—is thus to increase gradients of c at the boundary in order to facilitate the exchange of heat. In contrast to the typical internal mixing problem [22], where the concentration obeys homogeneous Neumann boundary conditions and the goal is to distribute passive scalar uniformly throughout the domain, there is no direct advantage here in increasing the gradients of c *inside* the domain. Hence optimal flows for the Dirichlet (transport) problem are unlikely to be the same as for the Neumann (mixing) problem. In any case the fundamental heat flux equation (4) is not obviously useful for direct optimization because it does not explicitly express how the velocity field $u(x)$ can enhance the flux.

Instead of focusing on the heat flux we can take a probabilistic approach. The *mean exit time* $T(x)$ is the expected time for a Brownian particle with diffusivity κ and drift $u(x)$ starting from $x \in \Omega$ to first hit the boundary of the domain $\partial\Omega$. The mean exit time satisfies a steady equation involving the adjoint of the operator on the right-hand side of (1):

$$(5) \quad 0 = u \cdot \nabla T + \kappa \Delta T + 1, \quad T = 0 \text{ on } \partial\Omega.$$

(See, for example, Redner [17, p. 31].) This looks like the steady advection-diffusion equation for a “concentration” $T(x)$ subject to flow $-u(x)$ with a constant source in the interior.

We expect that this mean exit time controls the cooling rate, since the process of cooling can be thought of as Brownian particles hitting the cold wall and exiting. Indeed, taking $(1) \times T - (5) \times c$ and integrating over space and time, we find after a few integrations by parts

$$(6) \quad \int_0^\infty \langle c \rangle(t) dt = \langle c_0 T \rangle,$$

where we used $c_0 = \int_0^\infty -\frac{\partial c}{\partial t} dt$ as the heat concentration decays at long times. Hölder's inequality then gives

$$(7) \quad \int_0^\infty \langle c \rangle(t) dt \leq \|c_0\|_p \|T\|_q, \quad p^{-1} + q^{-1} = 1,$$

for $p, q \geq 1$. In particular, for $p = 1$ and $q = \infty$, this can be written

$$(8) \quad \int_0^\infty \frac{\langle c \rangle(t)}{\langle c_0 \rangle} dt \leq \|T\|_\infty.$$

The quantity on the left can be interpreted as a “cooling time,” and we should aim to make it as small as possible for efficient heat exchange. The inequality (8) implies that the cooling time is at most the longest exit time over all initial Brownian particles. Thus, lowering $\|T\|_\infty$ should help cooling. This is impractical for many applications, since $\|T\|_\infty$ is often dominated by a very small volume. Moreover, the norm $\|T\|_\infty$ is notoriously difficult to optimize. A good compromise is to use $p = \infty, q = 1$ in (7), which gives

$$(9) \quad \int_0^\infty \langle c \rangle(t) dt \leq \|c_0\|_\infty \langle T \rangle,$$

where $\|T\|_1 = \langle T \rangle$ since $T \geq 0$. Thus, as long as $\|c_0\|_\infty$ is finite, lowering $\langle T \rangle$ will typically reduce the cooling time.

In this paper we shall focus on minimizing the integrated mean exit time $\langle T \rangle$ in order to achieve efficient heat exchange. We will do so via a direct variational approach, enforcing the constraint $\nabla \cdot u = 0$ and fixing the magnitude via a kinetic energy constraint

$$(10) \quad \frac{1}{2} \langle |u|^2 \rangle = (\kappa/L)^2 L^d \text{Pe}^2,$$

where Pe is a specific value of the Péclet number, L is a characteristic length scale, and d is the dimension of the space. We shall take $d = 2$ for the rest of the paper, but in principle our techniques apply to $d = 3$ with little modification.

2. An optimal exit time problem.

2.1. The variational problem. The problem considered here is the minimization of the mean exit time of Brownian particles from a bounded domain Ω , integrated over all initial conditions (i.e., the L^1 -norm of the mean exit time). Because $u \cdot n = 0$, escape from Ω ultimately relies on diffusion. In the absence of stirring ($u = 0$), the transport is purely conductive and the mean exit time depends solely on the fluid molecular diffusivity κ . However, as will be seen in section 2.2, stirring always lowers the integrated mean exit time for our problem. Note that this result is true for the L^1 -norm but not, for instance, the L^∞ -norm as demonstrated by [10], who proved

that for any 2D, simply connected domain different from a disk, there always exists a flow that *increases* the largest exit time compared to the pure conduction case (see Theorem 1.1 in [10]).

We nondimensionalize the problem such that $\kappa = L = 1$, which means that the length scale is L and the time scale is L^2/κ . We then define the advection-diffusion operator and its formal adjoint as

$$(11) \quad \mathcal{L} := u \cdot \nabla - \Delta, \quad \mathcal{L}^\dagger := -u \cdot \nabla - \Delta.$$

In the following we will consider a 2D domain, though our formulation easily works in three dimensions as well. We can then introduce a stream-function Ψ such that

$$(12) \quad u_x = -\frac{\partial \Psi}{\partial y} \quad \text{and} \quad u_y = \frac{\partial \Psi}{\partial x}.$$

We aim to determine the structure of the flow that realizes optimally efficient stirring, under a given energy constraint. From (5) and the energy constraint (10), the mean exit time and stream-function satisfy

$$(13a) \quad \mathcal{L}^\dagger T = 1,$$

$$(13b) \quad \langle |\nabla \Psi|^2 \rangle = 2\text{Pe}^2,$$

where we write \mathcal{L}^\dagger in terms of the Jacobian $J(a, b)$:

$$(14) \quad \mathcal{L}^\dagger T = -J(\Psi, T) - \Delta T, \quad J(a, b) := \partial_x a \partial_y b - \partial_y a \partial_x b.$$

We define the following functional, to be minimized in order to achieve minimal integrated mean exit time under the above constraints:

$$(15) \quad \mathcal{F}(T, \Psi, \Theta, \mu) = \langle T \rangle - \langle \Theta (\mathcal{L}^\dagger T - 1) \rangle + \frac{1}{2} \mu (\langle |\nabla \Psi|^2 \rangle - 2\text{Pe}^2),$$

where $\Theta(x)$ and μ are Lagrange multipliers. Extremizing the cost function \mathcal{F} under impermeability boundary conditions ($\Psi = 0$ on the wall) yields the Euler–Lagrange equations

$$(16a) \quad \mathcal{L}^\dagger T = 1,$$

$$(16b) \quad \mathcal{L} \Theta = 1,$$

$$(16c) \quad J(T, \Theta) - \mu \Delta \Psi = 0.$$

Observe that since \mathcal{L} is the advection-diffusion operator defined in (11), (16b) gives the temperature distribution Θ for a spatially uniform unit source of heat. There is thus a duality between the optimal exit time problem and the optimal heating problem, and the two are mapped to each other by reversing the velocity field. Put another way, under a fixed energy constraint, optimization of cooling in the internal heating problem and minimization of mean time in the exit time problem require solving the same set of Euler–Lagrange equations, the Lagrange multiplier in the first problem (16) satisfying the same equation as the passive scalar in the second one and vice versa. Solving for the exit time problem therefore provides a solution for the internal heating problem as well. We will focus on the former in the next sections, although the latter remains an underlying motivation as it may be relevant for many engineering purposes. It must be emphasized, however, that while solutions we obtain correspond at least to local extrema, we cannot guarantee whether they are global optima. Indeed, it remains an open challenge to prove that the mean exit time reduction realized by the flows constructed here are truly optimal by producing a rigorous lower bound with the same Pe dependence.

2.2. A judicious transformation. Let us introduce for convenience new variables η and ξ such that

$$(17) \quad T := T_0 + \frac{1}{2}(\eta + \xi) \quad \text{and} \quad \Theta := T_0 + \frac{1}{2}(\eta - \xi),$$

where $T_0(x)$ is the pure conduction solution ($u = 0$) in the domain:

$$(18) \quad -\Delta T_0 = 1.$$

In terms of these new variables, the Euler–Lagrange equations (16) become

$$(19a) \quad -J(\Psi, \xi) - \Delta \eta = 0,$$

$$(19b) \quad -J(\Psi, \eta) - \Delta \xi = 2J(\Psi, T_0),$$

$$(19c) \quad \frac{1}{2}J(\eta, \xi) + \mu \Delta \Psi = J(\xi, T_0),$$

to be solved under the energy constraint

$$(20) \quad \langle |\nabla \Psi|^2 \rangle = 2\text{Pe}^2,$$

and homogeneous Dirichlet boundary conditions for T , Θ , and Ψ on $\partial\Omega$.

As shown in Appendix A, the integrated mean exit time can be expressed as

$$(21) \quad \langle T \rangle = \langle T_0 \rangle - \frac{1}{4} \langle |\nabla \xi|^2 \rangle - \frac{1}{4} \langle |\nabla \eta|^2 \rangle.$$

Hence stirring always results in lowering the L^1 -norm for the mean exit time compared to the purely conductive case. The integrated mean exit time can also be expressed as (see Appendix A)

$$(22) \quad \langle T \rangle = \langle T_0 \rangle + \frac{1}{2} \langle \eta \rangle$$

or

$$(23) \quad \langle T \rangle = \langle T_0 \rangle - \text{Pe}^2 \mu - \frac{1}{4} \langle |\nabla \eta|^2 \rangle.$$

Both expressions will be of use later on.

3. Optimal stirring in a disk. From now on the domain is assumed to be a disk of radius 1 and cylindrical coordinates are adopted. Generalization to a broader range of geometries could be made following, for example, Alben [2], who used conformal mappings to extend to various geometries the results of [8] on optimal convection in a 2D channel. The pure conduction solution in the unit disk is $T_0 = \frac{1}{4}(1 - r^2)$ and the system (19) simplifies to

$$(24a) \quad -J(\Psi, \xi) - \Delta \eta = 0,$$

$$(24b) \quad -J(\Psi, \eta) - \Delta \xi = \frac{\partial \Psi}{\partial \theta},$$

$$(24c) \quad \mu \Delta \Psi = \frac{1}{2}J(\xi, \eta) + \frac{1}{2} \frac{\partial \xi}{\partial \theta},$$

with the kinetic energy constraint (20). We now seek some special nonlinear solutions of these equations.

3.1. The nonlinear ansatz. Inspired by linearized solutions, we try a nonlinear ansatz for solutions of (24) of the form

$$(25) \quad \eta = \eta(r), \quad \xi = \sqrt{2\mu} B(r) \cos m\theta, \quad \Psi = B(r) \sin m\theta,$$

with m an integer. Inserting this form into (24a) we obtain

$$(26) \quad (r\eta')' = BB'm\sqrt{2\mu},$$

which can be integrated once to give

$$(27) \quad r\eta' = m\sqrt{\mu/2} B^2,$$

where regularity of η at $r = 0$ was ensured by the choice of a zero integration constant. With the form (25), (24b) and (24c) are equivalent, and after using (27) they give a nonlinear eigenvalue problem for $B(r)$ with eigenvalue $\lambda := m/\sqrt{2\mu}$:

$$(28a) \quad r^2 B'' + rB' + (r^2\lambda - m^2)B = \frac{1}{2}m^2 B^3 \quad \text{with } B = 0 \text{ on } r = 0, 1.$$

To this must be appended the energy constraint (20):

$$(28b) \quad \frac{2\text{Pe}^2}{\pi} = \int_0^1 \left(B'^2 + \frac{m^2}{r^2} B^2 \right) r dr.$$

An analytical solution of (28) will be undertaken in the two asymptotic limits of small ($\text{Pe} \rightarrow 0$) and large Péclet number ($\text{Pe} \rightarrow \infty$).

3.2. Optimal stirring at low Pe. In the limit of small-energy flow, the cubic term can be omitted from (28a) and we recover a Bessel equation,

$$(29) \quad r^2 B'' + rB' + (r^2\lambda - m^2)B = 0.$$

For a given mode m , nonsingular solutions of (29) are proportional to the Bessel function $J_m(\sqrt{\lambda}r)$ whose positive roots determine the eigenvalue λ (and therefore the Lagrange multiplier μ) so as to meet the homogeneous Dirichlet boundary condition $B(1) = 0$:

$$(30) \quad \sqrt{\lambda} = j_{m,n}, \quad \mu = \frac{1}{2}m^2/j_{m,n}^4,$$

where $j_{m,n}$ is the n th positive root of the Bessel function J_m . We write $B = bJ_m$ in the energy constraint (28b) and use (29) to replace the integrand and obtain

$$(31) \quad \frac{2\text{Pe}^2}{\pi} = j_{m,n}^2 b^2 \int_0^1 r J_m^2(j_{m,n}r) dr.$$

Since $\int_0^1 r J_m^2(j_{m,n}r) dr = \frac{1}{2} J_m'^2(j_{m,n})$ [13], the amplitude of the solution is

$$(32) \quad b = \pm \frac{2\text{Pe}}{\sqrt{\pi} j_{m,n}} \frac{1}{J_m'(j_{m,n})}.$$

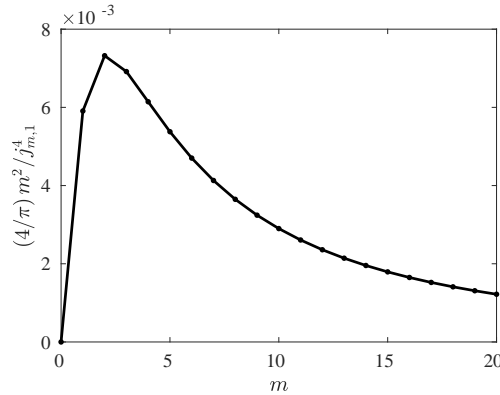


FIG. 1. The coefficient of Pe^2 in the small- Pe optimal enhancement (32) with $n = 1$ (first zero). The optimal enhancement is achieved for $m = 2$, then drops off slowly.

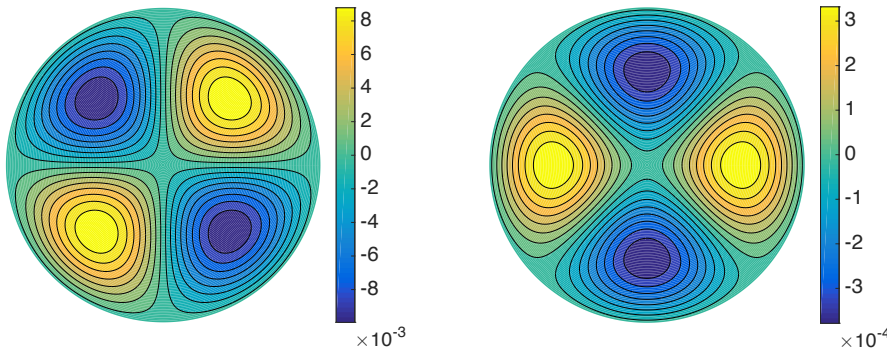


FIG. 2. Streamline pattern (left) and contours of the deviation from purely conductive mean exit time (right) for the optimal stirring flow at small Péclet ($Pe^2 = 0.001$) with $\xi + \eta = 0$ on the boundary.

The integrated mean exit time is given by (23), where $\langle T_0 \rangle = \frac{\pi}{8}$ for the unit disk. Since $B = O(Pe)$ and $\langle |\nabla \eta|^2 \rangle = O(Pe^4)$ following (27), this last contribution can be neglected in (23) and, using (30), we find

$$(33) \quad \frac{\langle T \rangle}{\langle T_0 \rangle} = 1 - \mu \frac{8Pe^2}{\pi} = 1 - \frac{4m^2}{\pi j_{m,n}^4} Pe^2.$$

Since $j_{m,n}$ increases monotonically with n , we must take $n = 1$ to minimize $\langle T \rangle$. Thus the optimal streamlines pattern displays a single cell in the radial direction. It is then a simple matter of enumerating the zeros $j_{m,1}$ to find that the integrated mean exit time is minimized for $(m, n) = (2, 1)$, independent of the Péclet number (see Figure 1). The streamline and mean exit time patterns are illustrated in Figure 2. Note that in this small- Pe limit the enhancement to the integrated mean exit time is small, so this is not a very practical regime for heat exchange.

4. Optimal stirring at large Pe and fixed m . In the previous section we derived Euler–Lagrange equations for optimal stirring in a disk and examined the small- Pe (linear) limit. The more relevant limit for actual heat exchangers is large Pe , since in this case stirring should greatly decrease the conductive integrated mean exit time and make the heat exchanger more efficient. However, the analysis is more complicated than in the linearized small- Pe limit and requires a boundary-layer approach.

4.1. Matched asymptotic solution. For a given mode m , let us first consider the asymptotic behavior of (28) at large energy. This requires a boundary layer approach, where the solution is relatively smooth in the bulk but exhibits rapid variations near the boundary. We give an outline of this approach here, and the details are relegated to Appendix B.

Large Pe is associated with fast flows, so we expect B to be large in (28a). In the bulk (away from the boundary layer), the cubic nonlinearity then dominates and can only be balanced by the eigenvalue λ scaling as B^2 . This results in $B(r) \sim r$ at leading order for the outer solution in the limit of infinitely large Pe , as long as r is not too small. A peripheral boundary layer, of thickness ε , accommodates the homogeneous Dirichlet boundary condition at $r = 1$, while local analysis reveals a behavior of $B \sim r^m$ near the origin, in a region whose typical thickness goes to 0 as Pe tends to infinity. (This internal layer exists for $m > 1$ only.) Neglecting this region as a first approximation, we form the composite solution

$$(34) \quad B = \sqrt{2\lambda/m^2} r \tanh((r-1)\sqrt{\lambda/2}).$$

(This is obtained by multiplying the linear outer solution (78) with the inner solution (81) and normalizing appropriately; the result is valid asymptotically both inside and outside the boundary layer.) Van Dyke's principle of least degeneracy [27], applied to the energy constraint (28b) after inserting (34), determines both $B = O(\text{Pe}^{2/3}) = O(\varepsilon^{-1})$ and the value of λ at leading order:

$$(35) \quad \lambda = (9m^4/2\pi^2)^{1/3} \text{Pe}^{4/3}.$$

The disk is split at radius $1-\delta$ with $\varepsilon \ll \delta \ll 1$ to separate the respective contributions of the inner and outer regions. Using (22), (27), and the approximation (34), the L^1 -norm of the mean exit time at fixed m , large Pe becomes at leading order

$$(36) \quad \langle T \rangle = (\pi^4/6)^{1/3} m^{-2/3} \text{Pe}^{-2/3},$$

as detailed in Appendix B. The calculation of the integrated mean exit time in (88) shows that the contribution of the conductive mean exit time $\langle T_0 \rangle = \pi/8 = O(1)$ is exactly canceled by the leading-order flow in the bulk (outer region). On the other hand, the remaining, leading-order integrated mean exit time $O(\varepsilon) = O(\text{Pe}^{-2/3})$ is solely determined by the peripheral boundary layer profile.

The large Pe , fixed m integrated mean exit time (36) correctly describes the asymptotic behavior of the solution for a given mode, as will be seen by comparing to numerical solutions in section 4.2. However, asymptotics at fixed m do not provide any evidence for the existence of an optimal flow pattern, since the integrated mean exit time goes to zero if m is chosen arbitrarily large. The optimal flow pattern results from a penalty on large wavenumbers m , associated with the $B \sim r^m$ dependence near the disk's origin, and arises from taking the distinguished limit for large m and large Pe . We will analyze this in detail in section 5.

4.2. Numerical results. For different values of the wavenumber m , we solve for the nonlinear eigenvalue problem (28) by means of a continuation method, using the MATLAB `bvp5c` function [19] with λ as a parameter. Starting from the Bessel function solution of section 3.2 as an initial guess in the quasi-linear regime (typically $\text{Pe}^2 = 10^{-3}$ – 10^{-1} depending on m), Pe is gradually increased up to $\text{Pe}^2 = 10^8$, the output of each computation providing an initial condition for the next one.

The numerical results are in excellent agreement with the asymptotics and reproduce the scaling (35) of $\lambda = O(\text{Pe}^{4/3})$. As can be seen in Figure 3, the numerical

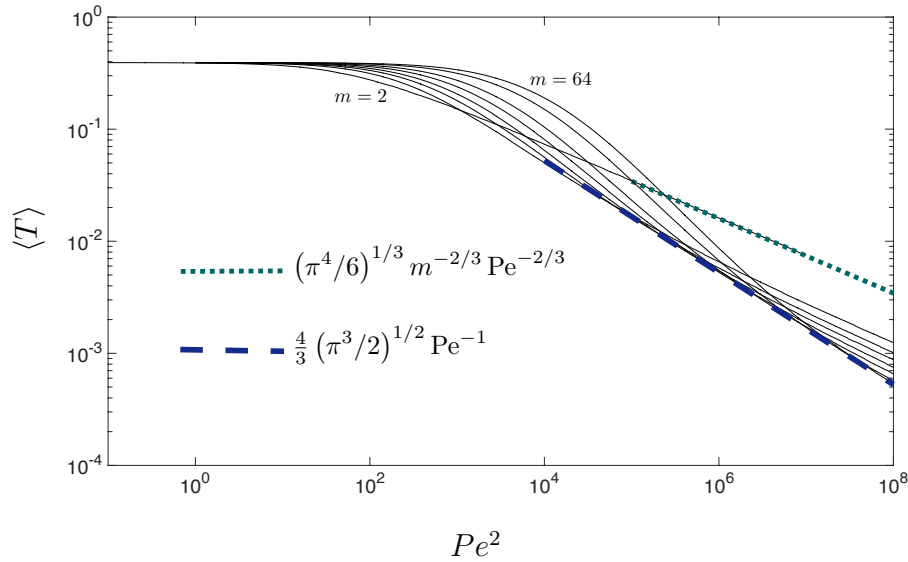


FIG. 3. Solid lines: numerical solution for the integrated mean exit time versus flow dimensionless energy Pe^2 , for the wavenumbers $m = \{2, 10, 14, 18, 24, 32, 48, 64\}$. Dotted line: large Pe , fixed m asymptotics, for $m = 2$. Dashed line: optimal integrated mean exit time (large Pe , large m asymptotics).

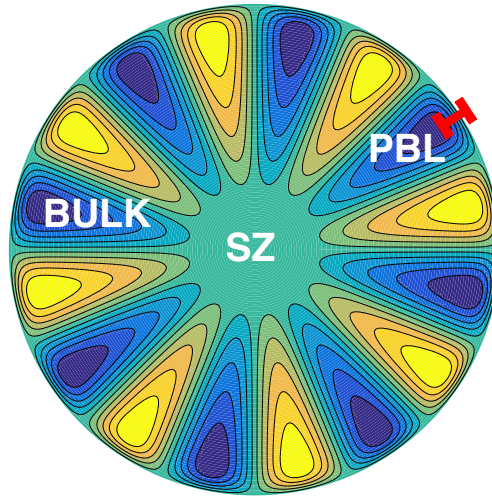


FIG. 4. Streamline pattern for $m = 8$, $Pe^2 = 1000$ (numerical solution of (28), obtained with *bvvp5c*). The different flow regions are SZ = internal boundary layer or “stagnation zone,” BULK = main flow, PBL = peripheral boundary layer.

integrated mean exit time for a given m perfectly superimposes with the large-energy asymptotics, provided Pe is large enough, with a decay $\sim Pe^{-2/3}$. A typical streamlines pattern is represented in Figure 4 for $m = 8$ and $Pe^2 = 10^3$. The superposition of integrated mean exit times for various wavenumbers in Figure 3 clearly indicates the existence of an optimal m at a given Pe : the minimal integrated mean exit time corresponds to the lower envelope of the various m graphs, whose equation satisfies a Pe^{-1} power law. In the next section we will find this optimal m as a function of Pe .

5. Optimal stirring at large Pe and large m . The penalty on large wavenumbers results from the presence of an internal layer (for $m > 1$): for large m , the streamlines of the incompressible flow strongly converge near the center of the disk where diffusion is likely to overpower radial transport. This creates a very-low-velocity region (a “stagnant” zone) which widens at fixed Pe with increasing m and shrinks with increasing Pe for fixed m . In this region, the flow is nearly ineffective and the mean exit time corresponds to the purely conductive one. Hence, for a given energy budget, an optimal flow has to be found by combining a large number of cells that efficiently expel particles toward the wall with a stagnation area of limited extent at the center of the disk. The signature of this competition between large- m -favored radial transport and the penalty associated with the growing stagnant zone can already be inferred from Figure 3 and motivates our search for an optimal value of m , which we will find to scale as $m \sim \text{Pe}^{1/2}$ below.

5.1. A composite solution for the large-Pe flow.

The outer solution (bulk). If we consider large wavenumbers and assume that m scales as some power of Pe, (28a) at leading order degenerates into

$$(37) \quad (\lambda r^2 - m^2) B = \frac{1}{2} m^2 B^3.$$

As in the fixed m case, balancing the eigenvalue and the cubic terms yields $\lambda r^2 \sim m^2 B^2$. The difference in the solution arises from the m^2 term on the left-hand side of (37), whose magnitude becomes comparable to the λr^2 term below a typical radius

$$(38) \quad r_{\times} := \sqrt{m^2/\lambda}.$$

The positive solution of (37) (outer solution) is then

$$(39) \quad B = \sqrt{2(r^2/r_{\times}^2 - 1)}.$$

This solution breaks down for a radius of $r \sim r_{\times}$, which is the typical thickness of the stagnation zone. Note that $r_{\times} \sim B^{-1}$, implying that the stagnation zone shrinks as the energy budget increases.

The inner solution ($r \rightarrow 1$). The homogeneous Dirichlet condition ($B = 0$ on $\partial\Omega$) is accommodated by a boundary layer on the wall. Writing ε the typical thickness of this peripheral layer, we rescale the radial coordinate as $r = 1 - \varepsilon\rho$. Expressing (28a) in the fast variable ρ yields

$$(40) \quad (1 - \varepsilon\rho)^2 \varepsilon^{-2} B'' + (1 - \varepsilon\rho) \varepsilon^{-1} B' + \lambda(1 - \varepsilon\rho)^2 B - m^2 B = \frac{1}{2} m^2 B^3,$$

and retaining the highest-order derivative in the dominant balance implies $\lambda \sim \varepsilon^{-2}$. Since $\lambda \sim m^2 B^2$ we have at leading order

$$(41) \quad \varepsilon^{-2} B'' + (\lambda - m^2) B = \frac{1}{2} m^2 B^3.$$

The solution of (41) (inner solution) satisfying the boundary condition in $r = 1$ (or $\rho = 0$) is

$$(42) \quad B = \sqrt{2(r_{\times}^{-2} - 1)} \tanh(k\rho),$$

where $k := \varepsilon \sqrt{\frac{1}{2}(\lambda - m^2)} = \varepsilon m \sqrt{\frac{1}{2}(r_{\times}^{-2} - 1)}$. This inner solution clearly matches asymptotically with the outer solution (39) as $\rho \rightarrow \infty$.

The stagnation zone (*internal layer*). Local analysis in the vicinity of the center reveals that $B \sim r^m$ as r goes to zero—the stirring there is largely ineffective. Thus the composite solution for B which is proposed in the next paragraph, where $B = 0$ is assumed everywhere in the stagnation zone, turns out to provide sufficient accuracy for the calculations to come. However, the asymptotic solution can be calculated also in the overlap region between the bulk and the stagnant zone, and for that purpose we introduce the change of variables $t := \ln(r/r_\times)$. Then (28a) becomes

$$(43) \quad B_{tt} + (\lambda r_\times^2 e^{2t} - m^2) B = \frac{1}{2} m^2 B^3.$$

Linearizing around $t = 0$ (or equivalently $r = r_\times = \sqrt{m^2/\lambda}$) yields at leading order

$$(44) \quad B_{tt} + 2m^2 t B = \frac{1}{2} m^2 B^3.$$

Straightforward rescaling of the variables transforms (44) to a Painlevé type II equation with zero constant:

$$(45) \quad b_{ss} = 2b^3 - sb,$$

where $s := (2m^2)^{1/3} \ln(r/r_\times)$. This equation does admit a particular solution—namely, the Hastings–McLeod solution b_{HM} (see [9], up to a change of sign $x \rightarrow -x$)—which asymptotically satisfies

$$(46) \quad b_{\text{HM}}(s) \underset{s \rightarrow -\infty}{\sim} \text{Ai}(s) \quad \text{and} \quad b_{\text{HM}}(s) \underset{s \rightarrow +\infty}{\sim} \sqrt{s/2},$$

thus displaying the correct behavior for $r \rightarrow 0$. Asymptotic matching with the bulk solution (39) takes care of itself as $r \rightarrow r_\times^+$; there the Hastings–McLeod solution becomes

$$(47) \quad B_{\text{HM}}(r) \sim 2 \sqrt{\ln \left(1 + \frac{r - r_\times}{r_\times} \right)} \sim 2 \sqrt{\frac{(r - r_\times)}{r_\times}},$$

to which the bulk solution (39) is also equivalent as $r \rightarrow r_\times$. Nevertheless, the calculation of the asymptotic integrated mean exit time in section 5.2 will be made considerably simpler by ignoring this last refinement and adopting the expression (48).

A composite solution. In the following, let us approximate the full solution by the composite solution

$$(48) \quad B \approx \begin{cases} \sqrt{2(r^2/r_\times^2 - 1)} \tanh[k\varepsilon^{-1}(1 - r)], & r > r_\times; \\ 0, & 0 < r < r_\times. \end{cases}$$

Indeed, comparison with the numerical solution of (28) in Figure 5 (obtained with MATLAB `bvp5c` using the continuation method described in section 4.2) shows excellent agreement, except for the small region restricted to the vicinity of r_\times (inset), which we shall neglect in what follows.

5.2. Optimal exit time at large Pe . Inserting (48) into the energy constraint (28b) and retaining only the leading-order terms yields a compact expression as a function of m and λ :

$$(49) \quad 2\text{Pe}^2/\pi \sim \lambda + \frac{2}{3} \sqrt{2\lambda^3/m^4}.$$

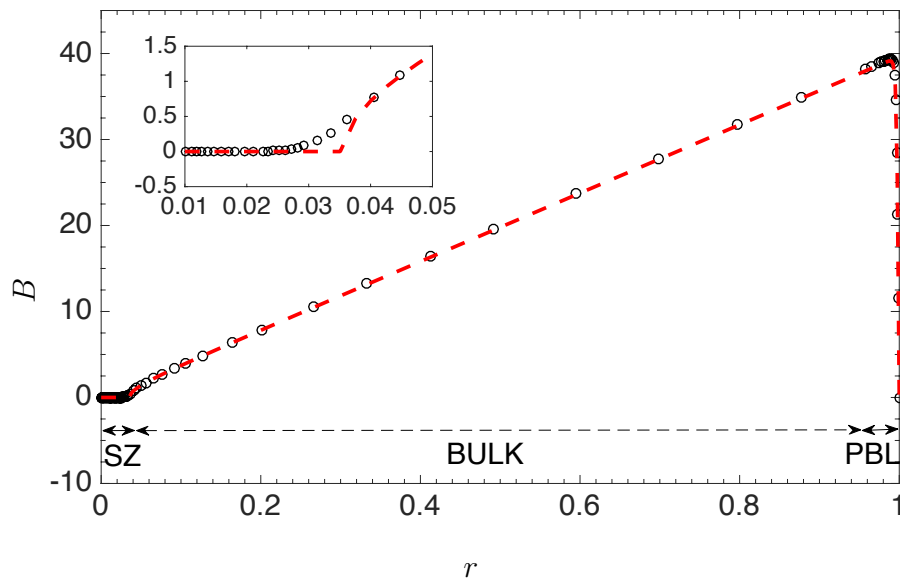


FIG. 5. Circles: numerical solution for $B(r)$ with $m = 16$, $Pe^2 = 8.4 \times 10^5$. Dashed line: approximated composite solution (48), where the eigenvalue $\lambda(m, Pe)$ is provided by the dispersion relation (49). Inset: blow-up in the vicinity of r_x . The different flow regions (SZ, BULK, PBL) correspond to those in Figure 4.

The details of the calculation parallel those for large Pe and fixed m from Appendix B; here we obtain an additional term λ compared to (85)–(86). Similarly, the integrated mean exit time at leading order is

$$(50) \quad \langle T \rangle \sim \frac{\pi}{4} m^2 \lambda^{-1} + \frac{\pi}{\sqrt{2}} \lambda^{-1/2},$$

which contains an additional term $m^2 \lambda^{-1}$ compared to (88). From the energy constraint (49) we can now deduce the scaling for m and λ from the requirement that all the terms be of the same order, which yields $m = O(Pe^{1/2})$ and $\lambda = O(Pe^2)$. This in turn determines the thickness of both the stagnation zone and the peripheral layer:

$$(51) \quad r_x = O(Pe^{-1/2}) \quad \text{and} \quad \varepsilon = O(Pe^{-1}).$$

(Recall that $\varepsilon = O(Pe^{-2/3})$ for the fixed- m case, so the boundary layer is thinner here.) Accordingly, let us renormalize the problem with $m = (2Pe^2/\pi)^{1/4} \tilde{m}$, $\lambda = (2Pe^2/\pi) \tilde{\lambda}$, and $\langle T \rangle / \langle T_0 \rangle = \frac{8}{\pi} \langle T \rangle = (2Pe^2/\pi)^{-1/2} \tilde{T}$. The energy constraint then becomes a dispersion relation between \tilde{m} and $\tilde{\lambda}$,

$$(52) \quad 1 \sim \tilde{\lambda} + \frac{2}{3} \sqrt{2} \tilde{\lambda}^{3/2} / \tilde{m}^2,$$

and the integrated mean exit time estimate is now

$$(53) \quad \tilde{T} \sim 2\tilde{m}^2 \tilde{\lambda}^{-1} + 4\sqrt{2} \tilde{\lambda}^{-1/2}.$$

For convenience we introduce the variable $Z := \tilde{\lambda}^{-1/2} \tilde{m}^2$. This allows the successive eliminations of $\tilde{\lambda}$ from (52) and then of both \tilde{m} , $\tilde{\lambda}$ from (53), yielding, respectively,

$$(54) \quad 1 \sim \tilde{m}^4 \left(Z^{-2} + \frac{2}{3} \sqrt{2} Z^{-3} \right) \quad \text{and} \quad \tilde{T} \sim \left(2Z + 4\sqrt{2} \right) \left(1 + \frac{2}{3} \sqrt{2} Z^{-1} \right)^{1/2}.$$

The asymptotic behavior of the conduction-normalized integrated mean exit time $\tilde{T}(Z)$ as $Z \rightarrow 0$ and $Z \rightarrow \infty$ already indicates the existence of a global minimum on \mathbf{R}_+ , which is obtained for

$$(55) \quad Z = \frac{2}{3}\sqrt{2}.$$

Therefore the flow parameters for optimal efficiency are

$$(56) \quad \tilde{m} = \sqrt{2/3} \quad \text{and} \quad \tilde{\lambda} = \frac{1}{2},$$

and hence

$$(57) \quad m = \sqrt{\frac{2}{3}} (2\text{Pe}^2/\pi)^{1/4} \quad \text{and} \quad \lambda = \frac{1}{2} (2\text{Pe}^2/\pi)^{3/4}.$$

For the optimal mode m , the optimal integrated mean exit time is then

$$(58) \quad \frac{\langle T \rangle}{\langle T_0 \rangle} \sim \frac{16}{3} \sqrt{2\pi} \text{Pe}^{-1} \quad \text{as } \text{Pe} \rightarrow \infty.$$

As can be seen in Figure 3, this is in excellent agreement with the numerical solutions of the eigenvalue problem (28) found with `bvp5c`: the dashed line corresponding to the asymptotic optimal integrated mean exit time perfectly matches the lower envelope of the different modes m for Pe^2 larger than approximately 10^4 .

6. Conclusions. The optimal integrated exit time (58) is expressed in terms of dimensionless quantities. Restoring dimensional units, this reads

$$(59) \quad \langle T \rangle \sim \frac{4}{3} \pi^{3/2} L^4 \langle |u|^2 \rangle^{-1/2} \quad \text{as } \text{Pe} \rightarrow \infty.$$

The scaling Pe^{-1} of (58) leads to a dimensional integrated mean exit time (59) that is *independent* of the molecular diffusivity: κ may be chosen arbitrarily small (but nonzero) and the particles will be expelled from the domain in purely mechanical time. (Once they reach the peripheral boundary layer, diffusivity is still needed for the particles to exit the domain.) This result is consistent with the bound on mixing efficiency derived in [23] at large Péclet number, which turns out to be independent of the molecular diffusivity (and is expected to hold under turbulent or chaotic mixing). Although our problem is different from the source optimization addressed in [24], and even though we use a different measure for quantifying the mixing efficiency (they consider the ratio of the L^2 -norms for the scalar concentration without and with stirring; see the case $p = 0$ in [24]), we can also recast (58) in terms of a “mixing enhancement factor”

$$(60) \quad \mathcal{E} = \frac{\langle T_0 \rangle}{\langle T \rangle} \sim \frac{3}{16\sqrt{2\pi}} \text{Pe} \quad \text{as } \text{Pe} \rightarrow \infty$$

and recover a similar linear dependence of the enhancement factor with Péclet number in the asymptotic $\text{Pe} \rightarrow \infty$ regime.

The sequence of flows we have constructed displaying this “mechanical time scaling” correspond to local extrema for the optimization problem, but we cannot guarantee that they are global extrema. Indeed, it remains an open challenge to prove that the mean exit time reduction realized by the flows constructed here is truly optimal by producing a rigorous upper bound on the enhancement with the same

Pe dependence. Moreover, our analysis also only hints qualitatively at what optimal flows might look like for domains with more complex shape: while we expect to see cells reaching into the domain and mechanical scaling for the enhancement for large Péclet number, we cannot predict the number or orientation of cells in general. Furthermore, the direct solution approach we have used here offers limited insight into optimal flow patterns and scalings for multiply connected domains, or for domains with mixed Neumann–Dirichlet boundaries.

It should also be emphasized that this analysis was performed assuming a steady flow under a fixed energy constraint, within a domain bounded by impermeable walls. Following [8], who studied optimal wall-to-wall transport of a passive scalar by a steady, incompressible flow in a channel, our analysis could be adapted for fixed enstrophy (fixed mean square vorticity) instead of energy budget, using stress-free boundary conditions. Hassanzadeh, Chini, and Doering [8] found maximal transport (as quantified by the Nusselt number Nu) to follow a power law $Nu \sim Pe$ in the large, fixed energy budget case (just as we found $\mathcal{E} \sim Pe$ for our minimal exit time problem), a scaling that becomes $Nu \sim Pe^{2/3}$ (possibly with logarithmic corrections) in the fixed enstrophy case [25]. Finally, it is unlikely that the flow achieving minimal exit time is a stationary one. The transient problem, namely, stirring optimization with a time-dependent flow achieving maximal mixing over a given time horizon (see, for example, [14]), is therefore another important challenge that remains to be addressed for engineering purposes.

Appendix A. A few useful identities. Let us prove first that our optimal solutions always lower the integrated mean exit time. Starting back from the original constraint (13a) and taking its scalar product by T yields

$$(61) \quad \langle |\nabla T|^2 \rangle = \langle T \rangle.$$

A similar operation on (18) yields for the conduction solution

$$(62) \quad \langle |\nabla T_0|^2 \rangle = \langle T_0 \rangle.$$

Using the decomposition (17), we write

$$(63) \quad \langle |\nabla T|^2 \rangle = \langle |\nabla T_0|^2 \rangle + \langle \nabla T_0 \cdot \nabla(\xi + \eta) \rangle + \frac{1}{4} \langle |\nabla(\xi + \eta)|^2 \rangle.$$

Taking the scalar product of (13a) by respectively T_0 and $(\xi + \eta)/2$ leads to

$$(64) \quad 0 = \langle T_0 J(\Psi, \xi + \eta) \rangle - \langle \nabla T_0 \cdot \nabla(\xi + \eta) \rangle,$$

$$(65) \quad 0 = \langle T_0 J(\Psi, \xi + \eta) \rangle + \frac{1}{2} \langle |\nabla(\xi + \eta)|^2 \rangle.$$

Thus

$$(66) \quad \langle \nabla T_0 \cdot \nabla(\xi + \eta) \rangle = -\frac{1}{2} \langle |\nabla(\xi + \eta)|^2 \rangle,$$

and, combining (63) with (66), (61), and (62),

$$(67) \quad \langle T \rangle = \langle T_0 \rangle - \frac{1}{4} \langle |\nabla(\xi + \eta)|^2 \rangle.$$

The last identity implies that *for any stirring flow* (however suboptimal), $\langle T \rangle \geq \langle T_0 \rangle$. Furthermore multiplying (19a) by ξ and integrating over the domain yields

$$(68) \quad \langle \nabla \xi \cdot \nabla \eta \rangle = 0,$$

hence the result (21).

We now derive two expressions for the L^1 -norm of the mean exit time. The scalar product of (19a), (19b), (19c) by, respectively, η , ξ , and Ψ yields

$$(69a) \quad \langle |\nabla\eta|^2 \rangle = \langle \eta J(\Psi, \xi) \rangle = \langle \Psi J(\xi, \eta) \rangle,$$

$$(69b) \quad \langle \eta J(\Psi, \xi) \rangle + \langle |\nabla\xi|^2 \rangle = 2 \langle \xi J(\Psi, T_0) \rangle,$$

$$(69c) \quad -\mu \langle |\nabla\Psi|^2 \rangle = \frac{1}{2} \langle \Psi J(\xi, \eta) \rangle + \langle \Psi J(\xi, T_0) \rangle.$$

After a few manipulations and use of the energy constraint (13b) we find

$$(70) \quad 4\mu \text{Pe}^2 = \langle |\nabla\xi|^2 \rangle,$$

which, combined with (67), (68), and (70), finally provides a convenient expression for $\langle T \rangle$:

$$(71) \quad \langle T \rangle = \langle T_0 \rangle - \mu \text{Pe}^2 - \frac{1}{4} \langle |\nabla\eta|^2 \rangle.$$

Moreover, we can also write

$$(72) \quad \langle T \rangle = \langle T_0 \rangle + \frac{1}{2} \langle \eta \rangle + \frac{1}{2} \langle \xi \rangle.$$

The scalar products of (16a) and (16b) by ξ yield, respectively,

$$(73a) \quad -\langle \xi J(\Psi, T) \rangle - \langle \xi \Delta T \rangle = \langle \xi \rangle,$$

$$(73b) \quad \langle \xi J(\Psi, \Theta) \rangle - \langle \xi \Delta \Theta \rangle = \langle \xi \rangle,$$

hence

$$(74) \quad 2 \langle \xi \rangle = -\langle \xi \Delta \eta \rangle - \langle \xi J(\Psi, \xi) \rangle = \langle \nabla\xi \cdot \nabla\eta \rangle = 0.$$

The latter, once combined with (72), provides an alternative expression for $\langle T \rangle$:

$$(75) \quad \langle T \rangle = \langle T_0 \rangle + \frac{1}{2} \langle \eta \rangle.$$

Appendix B. Large Pe, fixed m case. Let us consider the dominant balance in the bulk of the flow. In terms of the rescaled variables $B = \text{Pe}^\alpha \tilde{B}$ and $\lambda = \text{Pe}^\beta \tilde{\lambda}$, (28a) becomes

$$(76) \quad r^2 \tilde{B}'' \text{Pe}^\alpha + r \tilde{B}' \text{Pe}^\alpha + r^2 \tilde{\lambda} \tilde{B} \text{Pe}^{\alpha+\beta} - m^2 \tilde{B} \text{Pe}^\alpha = \frac{1}{2} m^2 \tilde{B}^3 \text{Pe}^{3\alpha}.$$

The only term that can balance the cubic is the one containing the eigenvalue, so we set $\beta = 2\alpha$. Thus at leading order (28a) degenerates into

$$(77) \quad r^2 \tilde{\lambda} \tilde{B} = \frac{1}{2} m^2 \tilde{B}^3,$$

which provides the outer solution

$$(78) \quad B_o = \text{Pe}^\alpha \tilde{B} = \pm \text{Pe}^\alpha \sqrt{2\tilde{\lambda}/m^2} r.$$

This solution does not meet the boundary condition $B(1) = 0$, which thus has to be accommodated by a boundary layer of thickness ε . Now introduce the stretched variable $\rho = (1-r)/\varepsilon$. The inner solution satisfies asymptotic matching with the outer solution, which suggests searching for $B = \text{Pe}^\alpha \bar{B}$ to get

$$(79) \quad \frac{(1-\varepsilon\rho)^2}{\varepsilon^2} \bar{B}'' \text{Pe}^\alpha + \frac{(1-\varepsilon\rho)}{\varepsilon} \bar{B}' \text{Pe}^\alpha + (1-\varepsilon\rho)^2 \tilde{\lambda} \bar{B} \text{Pe}^{3\alpha} - m^2 \bar{B} \text{Pe}^\alpha = \frac{1}{2} m^2 \bar{B}^3 \text{Pe}^{3\alpha}.$$

Dominant balance and the requirement that the highest-order derivative be retained yield $\varepsilon = O(\text{Pe}^{-\alpha})$, and (79) becomes at leading order:

$$(80) \quad \bar{B}'' + \tilde{\lambda}\bar{B} = \frac{1}{2}m^2 \bar{B}^3.$$

Asymptotic matching of the inner solution $\text{Pe}^\alpha \bar{B} = B_\infty \tanh(k\rho)$ with the outer solution as $\rho \rightarrow \infty$ yields $B_\infty = \pm \text{Pe}^\alpha \sqrt{2\tilde{\lambda}/m^2}$ and $k = \pm \sqrt{\tilde{\lambda}/2}$. At leading order the inner solution is then, up to a change of sign,

$$(81) \quad B_i = \text{Pe}^\alpha \sqrt{2\tilde{\lambda}/m^2} \tanh\left(\sqrt{\tilde{\lambda}/2} \rho\right).$$

The energy constraint (28b) determines α :

$$(82) \quad \frac{2\text{Pe}^2}{\pi} \sim \int_0^{1-\delta} \left(rB_o'^2 + \frac{m^2}{r} B_o^2 \right) dr + \int_{1-\delta}^1 \left(B_i'^2 + m^2 B_i^2 \right) dr,$$

where δ is an intermediate splitting scale ($\varepsilon \ll \delta \ll 1$). Using (78) and (81) yields

$$(83) \quad \frac{2\text{Pe}^2}{\pi} \sim \mathcal{F}_1 + \mathcal{F}_2 + \mathcal{F}_3$$

with

$$(84a) \quad \mathcal{F}_1 = \int_0^{1-\delta} B_\infty^2 r(1+m^2) dr = O(\text{Pe}^{2\alpha}),$$

$$(84b) \quad \mathcal{F}_2 = \int_{\delta\varepsilon^{-1}}^0 \frac{B_\infty^2 k^2}{\varepsilon} (1 - \tanh^2(k\rho))^2 d\rho = O(\text{Pe}^{2\alpha}\varepsilon^{-1}) = O(\text{Pe}^{3\alpha}),$$

$$(84c) \quad \mathcal{F}_3 = \int_{\delta\varepsilon^{-1}}^0 m^2 B_\infty^2 \varepsilon \tanh^2(k\rho) d\rho = O(\text{Pe}^{2\alpha}\varepsilon) = O(\text{Pe}^\alpha).$$

Dominant balance requires $\alpha = \frac{2}{3}$, hence $\beta = \frac{4}{3}$, meaning that the boundary layer thickness is of order $\text{Pe}^{-2/3}$. The leading terms in the energy constraint finally determine the eigenvalue $\lambda = \text{Pe}^{4/3}\tilde{\lambda}$:

$$(85) \quad \frac{2\text{Pe}^2}{\pi} \sim \mathcal{F}_2, \quad \text{i.e.,} \quad \frac{2}{\pi} \sim \int_{\delta\varepsilon^{-1}}^0 \frac{2\tilde{\lambda}k^2}{m^2} (1 - \tanh^2(k\rho))^2 d\rho,$$

which, using the identity $\tanh^2 - \tanh^4 = \tanh^2 \tanh'$ and recalling that $\delta \gg \varepsilon$, results in

$$(86) \quad \frac{2}{\pi} \sim \frac{2\sqrt{2}\tilde{\lambda}^{3/2}}{3m^2} \quad \text{hence} \quad \lambda \sim \text{Pe}^{4/3} \left(\frac{3m^2}{\pi\sqrt{2}} \right)^{2/3}.$$

The integrated mean exit time (22) can now be computed as

$$(87) \quad \langle T \rangle = \langle T_0 \rangle + \pi \int_0^1 r\eta dr = \langle T_0 \rangle - \frac{\pi}{2} \int_0^1 r^2 \eta' dr,$$

where we replace the integrand using (27), (78), and (81) to find

$$(88) \quad \langle T \rangle \sim \frac{\pi}{8} - \frac{\pi}{2} \int_0^{1-\delta} r^3 dr + \frac{\pi\varepsilon}{2k} \int_{k\delta\varepsilon^{-1}}^0 \tanh^2(u) du \sim \frac{\pi}{\sqrt{2\tilde{\lambda}}} \text{Pe}^{-2/3},$$

and finally

$$(89) \quad \langle T \rangle \sim \left(\frac{\pi^4}{6m^2} \right)^{1/3} \text{Pe}^{-2/3}.$$

Acknowledgments. The authors thank Stefan Llewellyn Smith for his assistance and advice during the GFD 2015 program in Woods Hole, as well as Gautam Iyer and Ian Tobasco for helpful discussions. This work originated at the 2015 Geophysical Fluid Dynamics program at the Woods Hole Oceanographic Institution.

REFERENCES

- [1] S. ALBEN, *Improved convection cooling in steady channel flows*, Phys. Rev. Fluids, 2 (2017), 104501.
- [2] S. ALBEN, *Optimal convection cooling flows in general geometries*, J. Fluid Mech., 814 (2017), pp. 484–509.
- [3] S. ARMAN, S. J. SMITH, D. A. SARTOR, R. E. BROWN, M. HERRLIN, J. G. KOOMEY, E. R. MASANET, N. HORNER, I. L. AZEVEDO, AND W. LINTNER, *United States Data Center Energy Usage Report*, Tech. Report LBNL-1005775, Lawrence Berkeley National Laboratory, Berkeley, CA, 2016.
- [4] G. C. DA GRAÇA, P. F. LINDEN, AND P. HAVES, *Design and testing of a control strategy for a large, naturally ventilated office building*, Building Serv. Eng. Res. Technol., 25 (2004), pp. 271–287.
- [5] J. DAI, M. OHADI, D. DAS, AND M. G. PECHT, *Optimum Cooling of Data Centers*, Springer, New York, 2014.
- [6] A. FAGHRI, *Heat pipes: review, opportunities and challenges*, Frontiers Heat Pipes, 5 (2014).
- [7] S. A. GAGE, G. R. HUNT, AND P. F. LINDEN, *Top down ventilation and cooling*, J. Architectural Planning Res., 18 (2001), pp. 286–301.
- [8] P. HASSANZADEH, G. P. CHINI, AND C. R. DOERING, *Wall to wall optimal transport*, J. Fluid Mech., 751 (2014), pp. 627–662.
- [9] M. HUANG, S.-X. XU, AND L. ZHANG, *Location of poles for the Hastings–McLeod solution to the second Painlevé equation*, Constr. Approx., 43 (2016), pp. 463–494.
- [10] G. IYER, A. NOVIKOV, L. RYZHIK, AND A. ZLATOŠ, *Exit times of diffusions with incompressible drift*, SIAM J. Math. Anal., 42 (2010), pp. 2484–2498.
- [11] Y. JOSHI AND P. KUMAR, *Energy Efficient Thermal Management of Data Centers*, Springer, New York, 2012.
- [12] S. KAKAÇ, H. YÜNCÜ, AND K. HIJIKATA, EDs., *Cooling of Electronic Systems*, Springer, New York, 1994.
- [13] N. N. LEBEDEV, *Special Functions and Their Applications*, Dover Publications, New York, 1972.
- [14] Z. LIN, C. R. DOERING, AND J.-L. THIFFEAULT, *Optimal stirring strategies for passive scalar mixing*, J. Fluid Mech., 675 (2011), pp. 465–476.
- [15] P. F. LINDEN, *The fluid mechanics of natural ventilation*, Annu. Rev. Fluid Mech., 31 (1999), pp. 201–238.
- [16] W. J. MINKOWYCZ, E. M. SPARROW, J. P. ABRAHAM, AND J. GORMAN, EDs., *Numerical Simulation of Heat Exchangers: Advances in Numerical Heat Transfer*, Vol. 5, Taylor and Francis, Philadelphia, 2017.
- [17] S. REDNER, *A Guide to First-Passage Processes*, Cambridge University Press, Cambridge, UK, 2001.
- [18] H. RONG, H. ZHANG, S. XIAO, C. LI, AND C. HU, *Optimizing energy consumption for data centers*, Renewable Sustainable Energy Rev., 58 (2016), pp. 674–691.
- [19] L. F. SHAMPINE, M. W. REICHEL, AND J. KIERZENKA, *Solving Boundary Value Problems for Ordinary Differential Equations in MATLAB with bvp4c*. <ftp://ftp.mathworks.com/pub/doc/papers/bvp> (2000).
- [20] A. K. D. SILVA, S. LORENTE, AND A. BEJAN, *Optimal distribution of discrete heat sources on a wall with natural convection*, Internat. J. Heat Mass Transfer, 47 (2004), pp. 203–214.
- [21] D. SONDAK, L. M. SMITH, AND F. WALEFFE, *Optimal heat transport solutions for Rayleigh–Bénard convection*, J. Fluid Mech., 784 (2015), pp. 565–595.
- [22] J.-L. THIFFEAULT, *Using multiscale norms to quantify mixing and transport*, Nonlinearity, 25 (2012), pp. R1–R44.

- [23] J.-L. THIFFEAULT, C. R. DOERING, AND J. D. GIBBON, *A bound on mixing efficiency for the advection-diffusion equation*, J. Fluid Mech., 521 (2004), pp. 105–114.
- [24] J.-L. THIFFEAULT AND G. A. PAVLIOTIS, *Optimizing the source distribution in fluid mixing*, Phys. D, 237 (2008), pp. 918–929.
- [25] I. TOBASCO AND C. R. DOERING, *Optimal wall-to-wall transport by incompressible flows*, Phys. Rev. Lett., 118 (2017), p. 264502.
- [26] A. I. UDDIN AND C. M. FEROZ, *Effect of working fluid on the performance of a miniature heat pipe system for cooling desktop processor*, Heat Mass Transfer, 46 (2009).
- [27] M. D. VAN DYKE, *Perturbation Methods in Fluid Mechanics*, Parabolic Press, Stanford, CA, 1975.
- [28] F. WALEFFE, A. BOONKASAME, AND L. M. SMITH, *Heat transport by coherent Rayleigh-Bénard convection*, Phys. Fluids, 27 (2015), 051702.